

Stably stratified air-flow over a waved water surface. Part 2: Wave-induced pre-turbulent motions

O. A. Druzhinin,^{a,b*} Y. I. Troitskaya^{a,b,c} and S. S. Zilitinkevich^{b,d,e,f,g}

^aInstitute of Applied Physics, Russian Academy of Sciences, Ul'yanova str. 46, Nizhny Novgorod 603950, Russia

^bRadiophysics Department, University of Nizhny Novgorod, Russia

^cInstitute of the Physics of Atmosphere, Russian Academy of Sciences, Moscow, Russia

^dPhysics Department, Moscow State University, Moscow, Russia

^eInstitute of Geography, Russian Academy of Sciences, Moscow, Russia

^fFinnish Meteorological Institute, Helsinki, Finland

^gDivision of Atmospheric Sciences, University of Helsinki, Finland

*Correspondence to: O. A. Druzhinin, Institute of Applied Physics, Russian Academy of Sciences, Ul'yanova str. 46, Nizhny Novgorod 603950, Russia. E-mail: druzhinin@hydro.appl.sci-nnov.ru

Recent experimental and direct numerical simulation (DNS) studies have discovered that stably stratified boundary-layer turbulence over a flat surface is characterized by the critical Reynolds number, Re_L , based on the Obukhov turbulent length-scale and the friction velocity, such that the transition from turbulent to laminar regime occurs at $Re_L \approx 10^2$. We have performed DNS of stably stratified flows over both flat and waved surfaces for a wide range of bulk Reynolds numbers and Richardson numbers and revealed that the same threshold, $Re_L = 10^2$, holds true over waved surfaces. However, when the surface wave slope is sufficiently steep, the supercritically stratified flow involves wave-induced, 'pre-turbulent' flow patterns, most pronounced in the vicinity of the waved water surface. In the present article, we study basic properties of these motions through DNS and propose a theoretical model of their generation via secondary parametric resonance instability of two-dimensional disturbances induced in the air-flow by the surface waves.

Key Words: stable stratification; boundary layer; waved water surface; wave-induced motions; direct numerical simulation

Received 26 March 2015; Revised 14 September 2015; Accepted 21 September 2015; Published online in Wiley Online Library

1. Introduction

Recent laboratory studies and direct numerical simulation (DNS) of stably stratified boundary-layer flows over flat, aerodynamically smooth surfaces have revealed the criterion of transition between turbulent and laminar regimes based on the turbulent Reynolds number:

$$Re_L = \frac{Lu_*}{\kappa\nu} > 100, \quad (1)$$

where ν is kinematic viscosity, $\kappa = 0.4$ is the von Kármán constant, u_* the friction velocity, and $L = -u_*^3/(F_t g/\Theta_0)$ is the Obukhov length-scale based on the vertical turbulent kinematic heat flux, F_t , gravitational acceleration g and a reference potential temperature Θ_0 (Flores and Riley, 2011). The steady-state turbulent regime is maintained at $Re_L > 10^2$ whereas at smaller Re_L turbulence degenerates and the flow becomes laminar. Further DNS of the stably stratified turbulent Couette flow over waved surfaces, performed by Druzhinin *et al.* (2015), Part 1 for a wide range of the bulk Reynolds and Richardson numbers, has revealed that the same critical value of the turbulent Reynolds number,

$Re_L = 10^2$, holds true for the flows over waved water surfaces. In the present article, we show that supercritically stratified flows over waves involve wave-induced disturbances, well-pronounced in the vicinity of the waved surface but weaker or even zero in the bulk of the flow domain. We also show that secondary instabilities of wave-induced 2D disturbances can cause formation of 'pre-turbulent' flow patterns, which become irregular for sufficiently steep waves and high Reynolds numbers. We consider in detail this pre-turbulent flow regime and suggest a theoretical interpretation of the origin of the observed pre-turbulent motions.

The design of DNS is the same as described by Druzhinin *et al.* (2015), Part 1. We consider a turbulent Couette flow above waved water surfaces in the Cartesian framework with the x -axis oriented along the mean wind, the z -axis oriented vertically upwards, and the y -axis parallel to the wave front, orthogonally to the mean flow. At the lower boundary, we prescribe a two-dimensional wave, periodic in the x -direction, with the amplitude a , wavelength λ and phase velocity c , and with wave slope up to $ka = 2\pi a/\lambda = 0.2$. DNS is performed in a reference frame moving with the wave phase velocity. The no-slip boundary conditions are prescribed at both the lower boundary, where the wind velocity coincides with the velocity of the water surface wave, and the

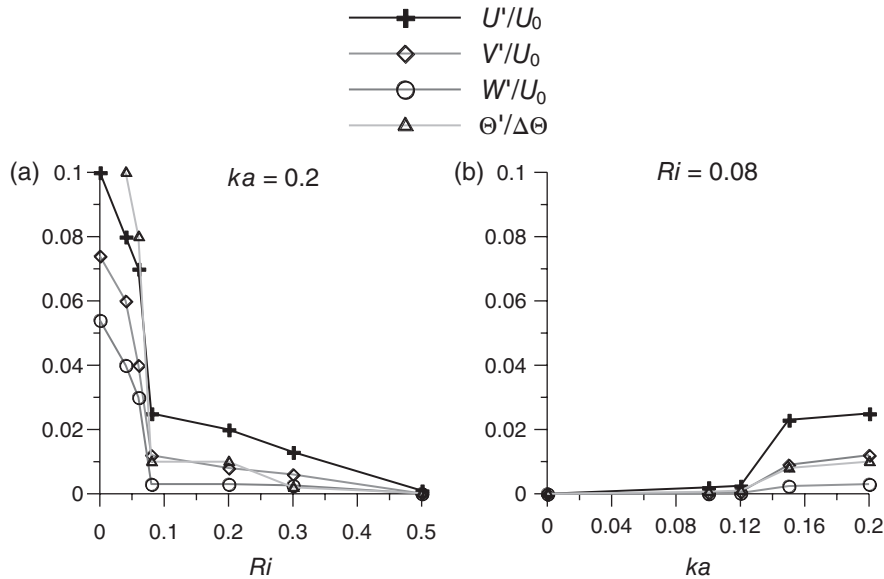


Figure 1. Root mean square fluctuations of the streamwise, transverse, and vertical velocity components, U' , V' and W' , and temperature, Θ' , as functions of (a) Richardson number, Ri , for constant wave slope, $ka = 0.2$, and (b) wave slope, ka , for $Ri = 0.08$, in DNS of stably stratified boundary-layer flows over wavy surfaces for $Re = 15\,000$.

upper boundary, which is defined as a horizontal plane moving in the x -direction with the bulk velocity U_0 . The computational domain has sizes $L_x = 6\lambda$, $L_y = 4\lambda$ and $L_z = \lambda$ in the x -, y -, and z -directions, respectively; and the wind flow is assumed to be periodic in the x - and y -directions. To establish the stable density stratification, we prescribe the temperatures Θ at the top and bottom boundary planes: $\Theta = \Theta_0$ at $z = 0$ and $\Theta = \Theta_0 + \Delta\Theta$ at $z = L_z$, where $\Delta\Theta > 0$.

The governing equations (full three-dimensional (3D) Navier-Stokes equations for incompressible fluid under the Boussinesq approximation) and the numerical method are described in detail by Druzhinin *et al.* (2015), Part 1). The governing parameters of the flow are the bulk Reynolds number:

$$Re = \frac{U_0 \lambda}{\nu} \quad (2)$$

and the bulk Richardson number:

$$Ri = g \frac{\Delta\Theta \lambda}{\Theta_0 U_0^2}, \quad (3)$$

where ν is kinematic viscosity of the air. The Prandtl number, $Pr = \nu/\mu$ (where μ is thermal diffusivity), is prescribed as $Pr = 0.7$. Numerical simulations are performed for Re and Ri in the range $15\,000 < Re < 80\,000$ and $0 < Ri < 0.3$, the wave slope in the range $0 < ka < 0.2$, and different values of the phase velocity, c .

DNS is performed in dimensionless coordinates: $x_1 = x/\lambda$, $x_2 = y/\lambda$, and $x_3 = z/\lambda$ and dimensionless variables: temperature deviation from the reference temperature, $\tilde{T} = [\Theta - \Theta_{ref}]/\Delta\Theta$, and x -, y -, and z -velocity components, $U_1 = U_x/U_0$, $U_2 = U_y/U_0$, and $U_3 = U_z/U_0$ (cf. Druzhinin *et al.*, 2015, Part 1).

A conformal mapping is employed, which transforms the Cartesian coordinates (x_1, x_3) into curvilinear coordinates (ξ, η) , in which the wavy surface becomes the flat plane ($\eta = 0$). The numerical grid is clustered in the vertical direction to provide sufficient resolution of the flow near both bottom and top boundary planes. The velocity field at the initial moment, $t = 0$, is prescribed as a weakly perturbed laminar Couette flow; and the initial temperature deviation from the reference profile is taken to be 0. The sampling of the velocity and temperature fields is performed at sufficiently late times when the stationary turbulence regime sets in. The time averaging is performed during the period when the flow has reached the statistically stationary state, whereas averaging over the wavelength is performed as the window-averaging. For a given field $f(x_1, x_2, x_3, t)$, the phase

average, $\langle f \rangle(x_1, x_3)$, and the dispersion, $\langle f^2 \rangle(x_1, x_3)$, are obtained by the averaging over the wavelength in the x_1 -direction, along the wave front in the x_2 -direction, and in time; the root mean square fluctuation is obtained as:

$$f' = ([\langle f^2 \rangle] - [\langle f \rangle]^2)^{1/2}. \quad (4)$$

The mean vertical profile, $[\langle f \rangle](x_3)$, is obtained by additional averaging of the phase-averaged field over the streamwise coordinate x_1 . Thus, vertical profiles of mean turbulent fluxes of momentum and heat, $\tau(x_3)$ and $F(x_3)$, are determined as

$$\tau(x_3) = [\langle U_1 U_3 \rangle] - \langle U_1 \rangle \langle U_3 \rangle, \quad (5)$$

$$F(x_3) = [\langle U_3 \tilde{T} \rangle] - \langle U_3 \rangle \langle \tilde{T} \rangle. \quad (6)$$

2. Basic features of the wave-induced pre-turbulent motions revealed from DNS

Figure 1 shows the maxima of the root mean square velocity and temperature fluctuations (U' , V' , W' and Θ') as:

$$U', V', W' \equiv U_0 \max\{U'_i\}, i = 1, 2, 3; \Theta' \equiv \Delta\Theta \max\{\tilde{T}'\} \quad (7)$$

(where U'_i and \tilde{T}' are obtained as described in Eq. (4)) versus Ri for the wave slope $ka = 0.2$, and versus ka for $Ri = 0.08$, obtained in DNS for $Re = 15\,000$. At the given wave slope $ka = 0.2$, the developed turbulence regime and wave-induced pre-turbulence regime are separated by the threshold bulk Richardson number $Ri_{th} \approx 0.07$ (Figure 1(a)); whereas at the given $Ri = 0.08$ these regimes are separated by the threshold wave slope $ka_{th} \approx 0.14$ (Figure 1(b)). Figure 1(a) shows that the rms values are drastically (by an order of magnitude) reduced under the pre-turbulent regime compared to the turbulent regime for $Ri > 0.07$. On the other hand, Figure 1(b) shows that the occurrence of the pre-turbulent regime is also characterized by a threshold value of the wave slope ($ka \approx 0.12$) so that, for fixed supercritical $Ri > Ri_{th}$ and sufficiently small ka (i.e. $ka < 0.12$), the fluctuations vanish, and the pre-turbulent regime is not observed.

Figure 2 shows instantaneous fields of the vorticity modulus, $\omega(x, y, z)$, in different cross-sections of the flow, obtained for $Re = 15\,000$, $Ri = 0.08$, $ka = 0.2$ and $c/U_0 = 0.05$, at time $t = 1000$. The figure shows that pre-turbulent fluctuations are quite pronounced in the vicinity of the wavy surface, where the

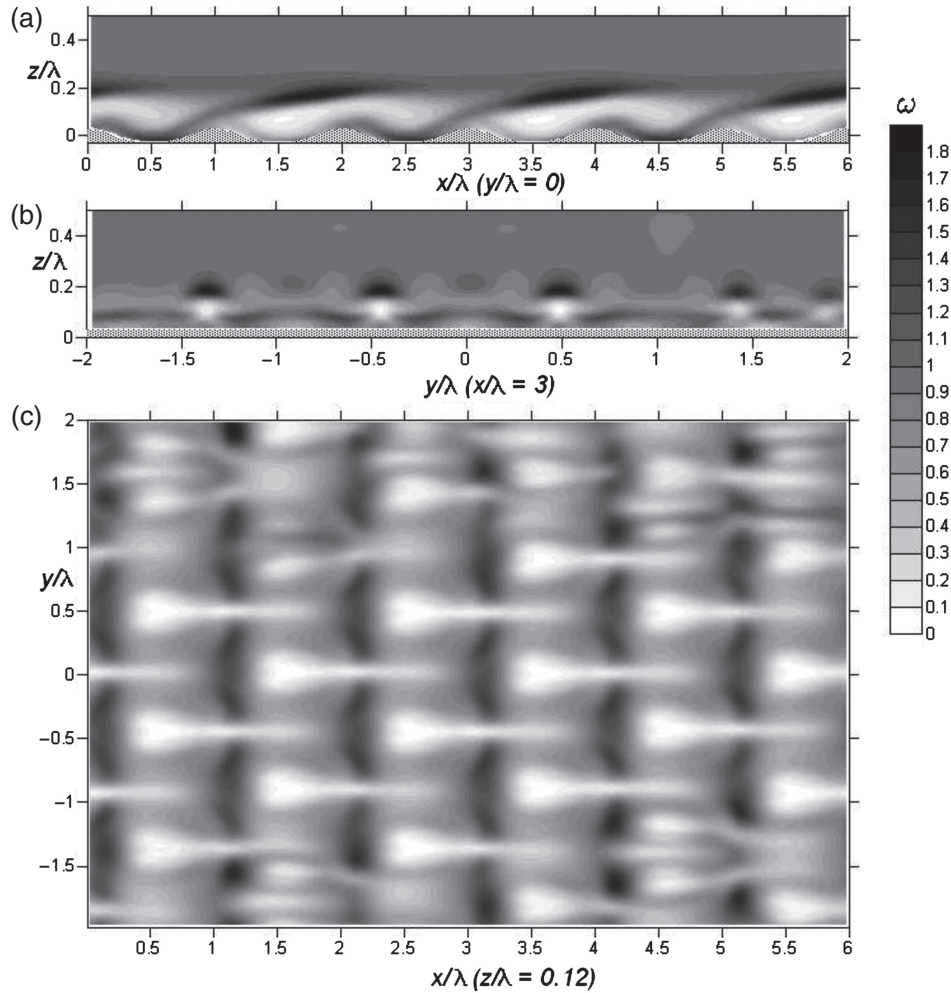


Figure 2. Instantaneous field of the vorticity modulus in (a) the x,z plane at $y=0$, (b) the y,z plane at $x=3$ and (c) the x,y plane at $z=0.12$, obtained from DNS of the wave-induced pre-turbulence in stably stratified boundary-layer flows for the bulk Reynolds number $Re = 15\,000$, bulk Richardson number $Ri = 0.08$, wave slope $ka = 0.2$, and dimensionless phase velocity $c/U_0 = 0.05$, at time $t = 1000$.

vorticity field exhibits a complicated 3D structure, and these fluctuations decay sufficiently far from the surface.

Figure 3 shows dimensionless vertical profiles of the mean velocity, $U(z)/U_0$, deviation of the mean temperature from its surface value, $(\Theta(z) - \Theta_0)/\Delta\Theta$, root mean square fluctuations of velocity and temperature (U' , V' , W' and Θ'), Eq. (7), and momentum and heat fluxes, Eqs (5) and (6), obtained for $Ri = 0.08$ at the phase velocities $c/U_0 = 0.05$ and $c/U_0 = 0.2$. Maximal fluctuations and momentum fluxes in the wave-induced pre-turbulent regime are observed in the vicinity of the critical level $z = z_c$, defined as the height where the wind velocity coincides with the wave phase velocity: $U(z_c) = c$. In DNS under consideration, the critical level is $z_c \approx 0.1 \lambda$ for $c/U_0 = 0.05$ (a,b,c) and $z_c \approx 0.4 \lambda$ for $c/U_0 = 0.2$ (d,e,f). In the case $c/U_0 = 0.05$, the heat flux, $(-c U' \Theta')$, turns to 0 at the critical level, is positive above z_c and negative below z_c (cf. Figure 3(c)). On the other hand, the heat flux is positive and has maximum at the critical level for $c/U_0 = 0.2$ (Figure 3(f)). Figure 3 shows that, under the pre-turbulent regime, increasing wave speed reduces the momentum flux and increases the heat flux.

Figure 3(a,d) also demonstrate vertical profiles of the gradient Richardson number:

$$Ri_g = \frac{g}{\Theta_0} \frac{d\Theta/dz}{(dU/dz)^2} = \frac{N^2}{(dU/dz)^2}, \quad (8)$$

where $N(z)$ is the buoyancy frequency. In both cases, Ri_g has maximum at the critical layer and does not exceed the critical value, $Ri_g = 0.25$, at all heights for $c/U_0 = 0.05$ (a) and at the heights $z > 0.05$ for $c/U_0 = 0.2$ (d). In both cases, Ri_g increases rapidly in the vicinity of the boundary, for $z < 0.05$.

Figure 4 presents instantaneous power spectrum, $E(k_x, k_y)$, obtained by the Fourier transform of the vorticity field in the horizontal (x, y) plane shown in Figure 2. The spectrum exhibits peaks at the wavenumbers $\mathbf{k} = (2\pi, 0)$, $\mathbf{k}_1 = (\pi, 2\pi)$, $\mathbf{k}_2 = (4\pi, 0)$ and $\mathbf{k}_3 = (0, 4\pi)$. The peak at $\mathbf{k} = (2\pi, 0)$ corresponds to the two-dimensional (2D) disturbance directly induced in the air-flow by the surface wave. However, the 2D forcing alone would not be able to directly produce a 3D disturbance, heterogeneous in the y -direction along the surface-wave front and characterized by the energy peaks at wavenumbers \mathbf{k}_1 and \mathbf{k}_3 . Below in the section 3, we show that the 3D structure of the vorticity field in the horizontal (x,y)-plane in Figure 2 and the spectral peak at the wavenumber $\mathbf{k}_1 = (\pi, 2\pi)$ can be regarded as a consequence of the development of a secondary instability of the 2D wave-induced disturbances, caused by nonlinear wave interaction. Additional peaks at wave numbers \mathbf{k}_3 and \mathbf{k}_4 in the spectrum $E(k_x, k_y)$ may result from nonlinear generation of second harmonics.

In order to investigate the effect of increasing the bulk Reynolds number, Re , on the wave-induced pre-turbulent motions, we performed DNS for fixed values of $Ri = 0.2$ and $c/U_0 = 0.05$ and different sets of other governing parameters: $Re = 40\,000$, $ka = 0.2$, and $Re = 80\,000$, $ka = 0.15$. The numerically simulated instantaneous fields of the vorticity modulus in the horizontal (x,y)-plane at $z = 0.12$ for $Re = 40\,000$ (a) and $Re = 80\,000$ (b) are shown in Figure 5 and the corresponding 2D spectra are shown in Figure 6. As illustrated, the flows with the larger bulk Reynolds numbers: 15 000, 40 000 and 80 000 exhibit the more complicated spatial structures. At $Re = 80\,000$, new peaks are formed and some peaks merge, which is indicative of widening the spectrum, hence the complication of the pre-turbulence and its development towards real turbulence.

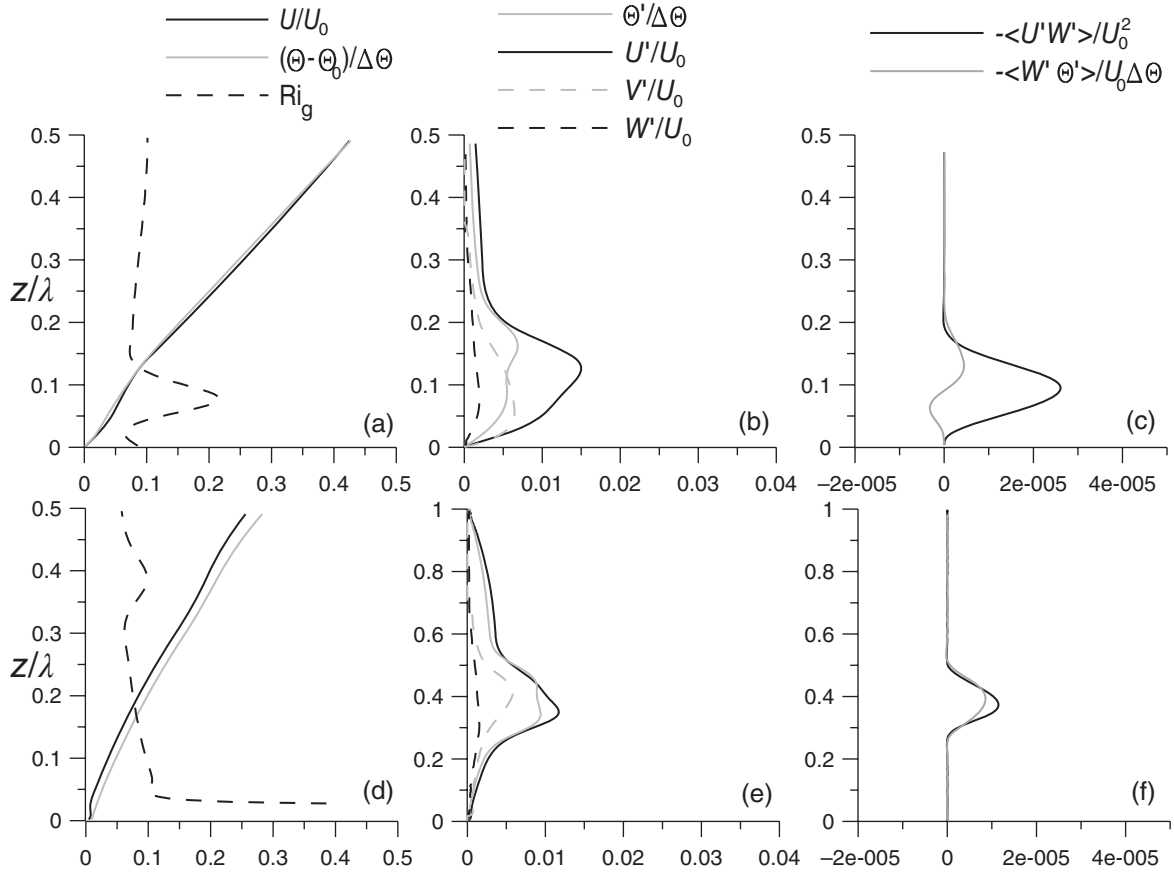


Figure 3. Vertical profiles of (a, d) the mean velocity and temperature and the gradient Richardson number, (b, e) the velocity and temperature fluctuations, and (c, f) the momentum and heat fluxes in DNS of the wave-induced pre-turbulent flow over waved surface with $ka = 0.2$ and (a,c) $(ac/U_0 = 0.05$ and (d,f) $c/U_0 = 0.2$, for $Re = 15\,000$ and $Ri = 0.08$.

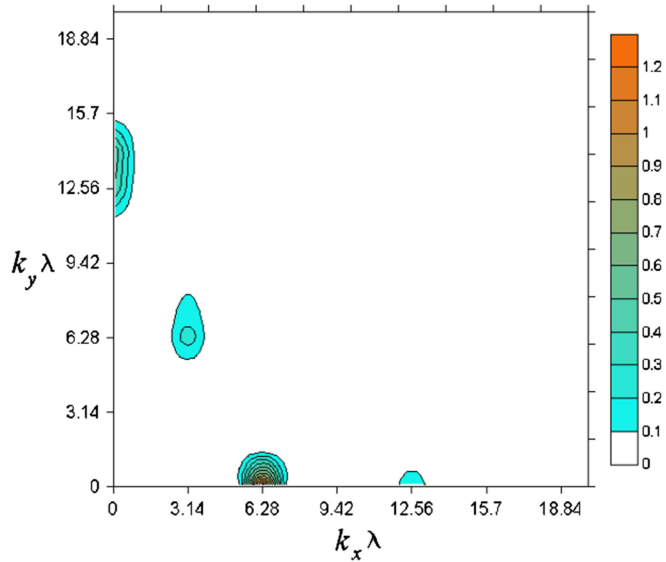


Figure 4. Instantaneous power spectrum of the vorticity field in pre-turbulent air flow over the waved water surface for $c/U_0 = 0.05$, $Re = 15\,000$, $Ri = 0.08$ and $ka = 0.2$ (the case shown in Figure 2 on the x, y plane at $z = 0.12$).

3. The resonant mechanism of secondary instability

In this section, we develop a theoretical model explaining the mechanism of the generation of wave-induced disturbances in super-critically stratified air-flow above the waved water surface revealed in our DNS. The basic physical mechanism is identified as follows. The wave on the water surface induces a 2D disturbance in the air-flow which has the same wave number and phase velocity as the surface water wave. This 2D disturbance is subjected to a secondary instability that, in turn, leads to the generation of the

3D structure of the flow revealed in DNS in the vorticity field shown in Figure 2.

To evaluate the velocity and temperature fluctuations in the 2D disturbance directly forced by the surface wave, we use 2D Navier-Stokes equations, written under the Boussinesq approximation, in curvilinear coordinates:

$$x = \xi - a \exp(-k\eta) \sin k\xi, \quad (9)$$

$$z = \eta + a \exp(-k\eta) \cos k\xi, \quad (10)$$

in terms of vorticity χ , stream function ψ and temperature Θ (Troitskaya *et al.* (2013a, 2013b)). We consider a 2D base flow with the velocity and temperature profiles coinciding with the steady-state mean velocity and temperature profiles in DNS, $U(\eta)$ and $\Theta(\eta)$. The 2D fluid-motion equations are recast in terms of the vorticity and stream function with base profiles, $\chi_0(\eta)$ and $\psi_0(\eta)$, defined by:

$$\chi_0(\eta) = \frac{dU}{d\eta}, \quad \psi_0(\eta) = \int_0^\eta (U(\eta') - c) d\eta'. \quad (11)$$

Further we consider the vorticity, streamfunction and temperature as sums of the base profiles and 2D disturbances forced by the surface wave:

$$\begin{aligned} \chi(\eta, \xi) &= \chi_0(\eta) + \Re\{\chi_1(\eta) \exp(ik\xi)\}, \\ \psi(\eta, \xi) &= \psi_0(\eta) + \Re\{\psi_1(\eta) \exp(ik\xi)\}, \\ \Theta(\eta, \xi) &= \Theta(\eta) + \Re\{\Theta_1(\eta) \exp(ik\xi)\}, \end{aligned} \quad (12)$$

where $\Re\{\dots\}$ denotes the real part of the expressions in curly brackets. The equations for disturbances are obtained by substitution of Eq. (12) into the 2D Navier-Stokes equations and linearization with respect to χ_1 , ψ_1 , and Θ_1 . The resulting

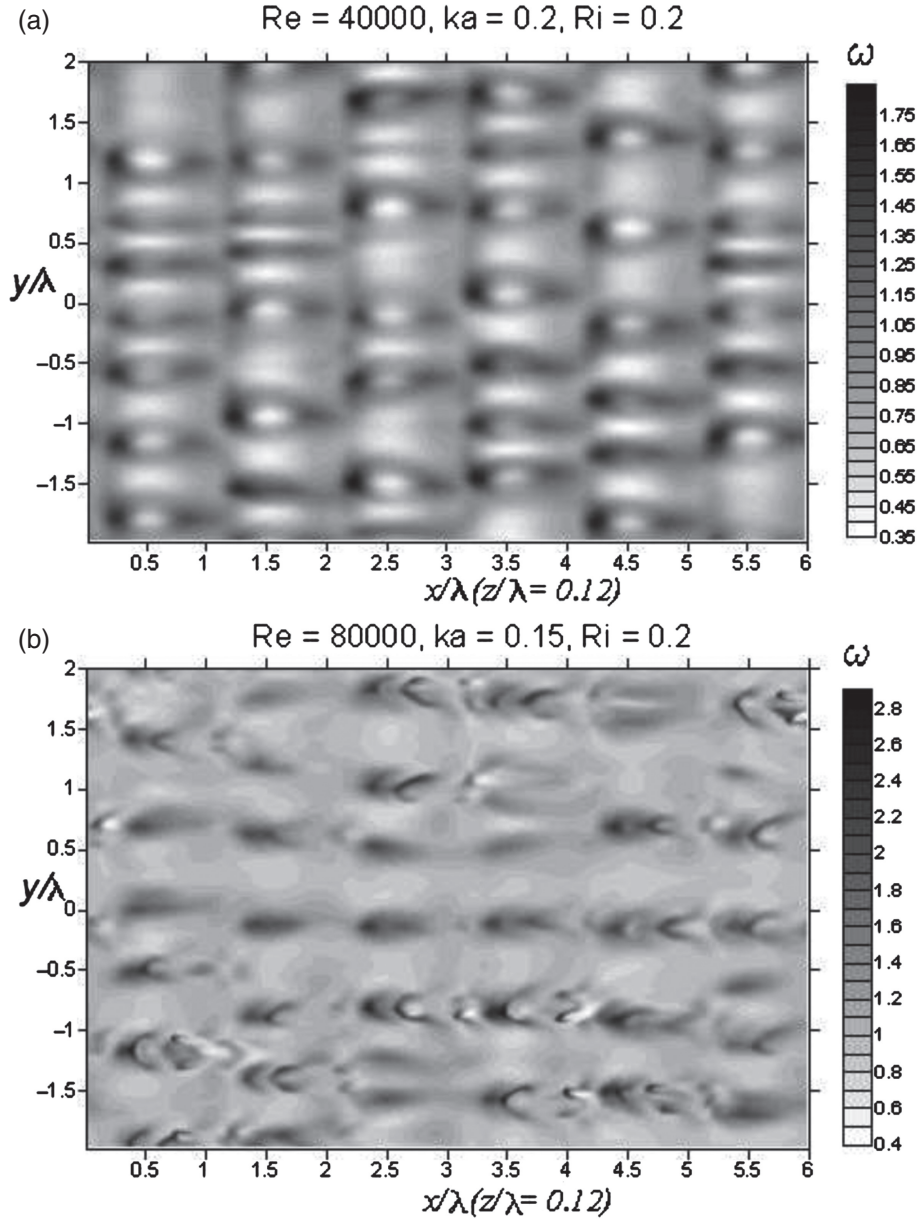


Figure 5. Instantaneous field of the absolute value of vorticity in the horizontal plane (x, y) at $z = 0.12$ obtained in DNS for (a) $Re = 40\,000$, $Ri = 0.2$, $ka = 0.2$ and (b) $Re = 80\,000$, $Ri = 0.15$, $ka = 0.15$, both at the phase velocity $c/U_0 = 0.05$ and at time $t = 600$.

equations can be written in the curvilinear coordinates (ξ, η) in the form (Troitskaya *et al.* (2013a, 2013b)):

$$ik \left(\frac{d\psi_0}{d\eta} \chi_1 - \frac{d\chi_0}{d\eta} \psi_1 \right) - \frac{ikg}{\Theta_0} \left(\Theta_1 - a \frac{d\Theta}{d\eta} e^{-k\eta} \right) = \nu \left(\frac{d^2 \chi_1}{d\eta^2} - k^2 \chi_1 \right), \quad (13)$$

$$\frac{d^2 \psi_1}{d\eta^2} - k^2 \psi_1 = \chi_1 - 2ake^{-k\eta} \chi_0, \quad (14)$$

$$ik \left(\frac{d\psi_0}{d\eta} \Theta_1 - \frac{d\Theta}{d\eta} \psi_1 \right) = \frac{\nu}{Pr} \left(\frac{d^2 \Theta_1}{d\eta^2} - k^2 \Theta_1 \right). \quad (15)$$

Equations (13–15) are supplemented by the boundary conditions at the water surface in the form:

$$\psi_1|_{\eta=0} = 0, \quad \left. \frac{d\psi_1}{d\eta} \right|_{\eta=0} = 2cka, \quad \Theta_1|_{\eta=0} = 0. \quad (16)$$

Conditions in Eq. (16) are the impermeability condition of the water surface with respect to the air, the ‘no-slip’ at the water surface, and vanishing temperature deviation at the water

surface, respectively. It is also assumed that all disturbances vanish sufficiently far from the water surface:

$$\psi_1|_{\eta \rightarrow \infty} = 0, \quad \left. \frac{d\psi_1}{d\eta} \right|_{\eta \rightarrow \infty} = 0, \quad \Theta_1|_{\eta \rightarrow \infty} = 0. \quad (17)$$

Figure 7 shows vertical profiles of the r.m.s. fluctuations of the horizontal and vertical velocity and temperature, calculated from Eqs (13)–(15), where the mean velocity and density profiles are taken from DNS for $Re = 15\,000$, $Ri = 0.08$, $ka = 0.2$, and $c = 0.05$. These theoretically calculated r.m.s. fluctuation profiles are compared with profiles of the same fluctuation taken directly from our DNS of the wave-induced, phase-averaged velocity and temperature fields:

$$\begin{aligned} U'_w &= U_0([\langle U_1 \rangle^2] - [\langle U_1 \rangle]^2)^{1/2}, \\ W'_w &= U_0([\langle U_3 \rangle^2] - [\langle U_3 \rangle]^2)^{1/2}, \\ \Theta'_w &= \Delta\Theta([\langle \tilde{T} \rangle^2] - [\langle \tilde{T} \rangle]^2)^{1/2}. \end{aligned} \quad (18)$$

The figure shows a good agreement between the model and DNS. The observed differences can be attributed to development of inhomogeneous motions in the y -direction, along the surface wave crest. It is conceivable that the low-mode, almost regular

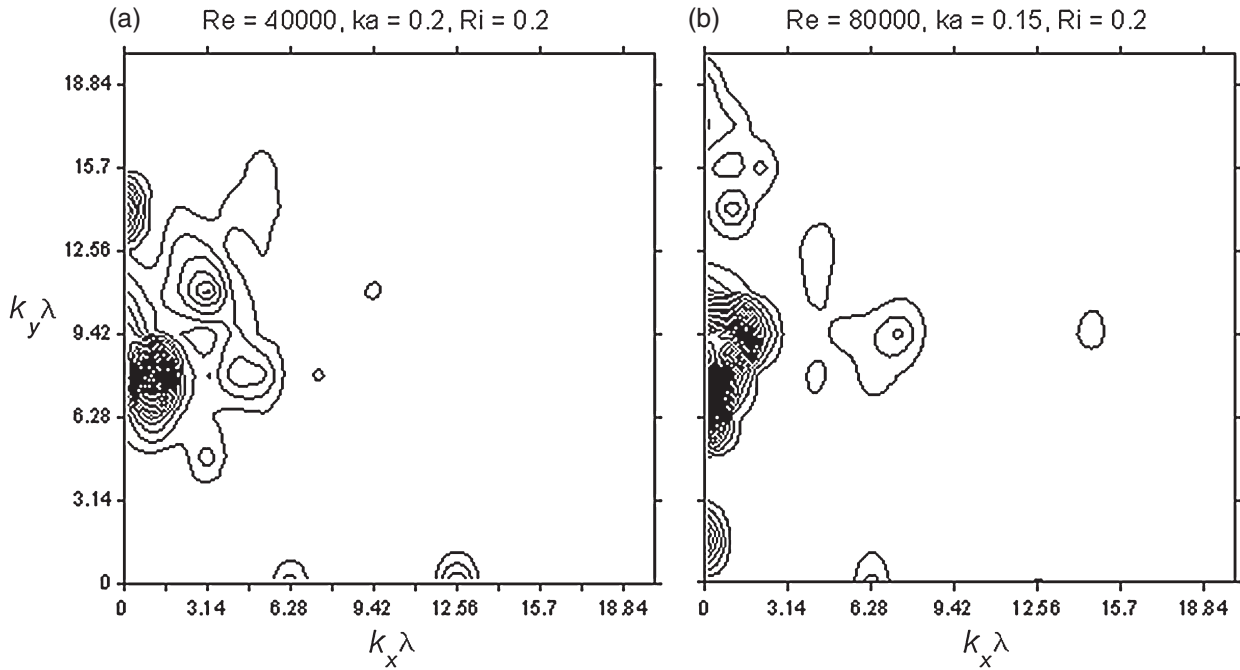


Figure 6. Instantaneous power spectra of the vorticity fields shown in Figure 5. The increments between the lines are (a) 0.05 and (b) 0.02.

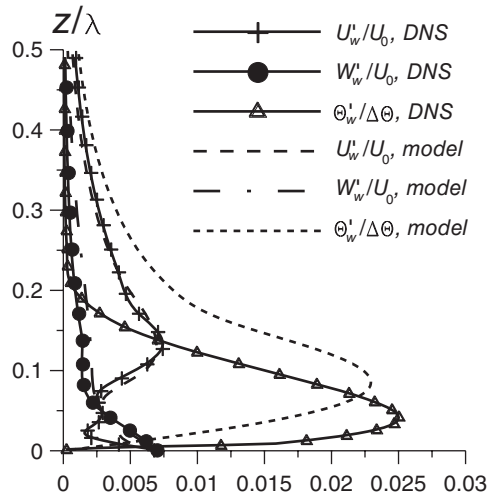


Figure 7. Wave-induced velocity and temperature disturbances in DNS (solid lines) and theoretical model (dashed lines).

flow pattern in Figure 2 is caused by interaction of the basic wave, with the wave number $\mathbf{k} = (2\pi, 0)$, with oblique waves, with wave numbers $\mathbf{k}_1 = (\pi, \pm 2\pi)$, via a parametric resonance mechanism (cf. Figure 4).

Craik (1971) has already considered a comparable mechanism to explain the secondary instabilities in the boundary layer over a flat plate. Our case is essentially different. First, the main disturbance is the forced wave-induced disturbance, and its amplitude is maintained constant, whereas in Craik (1971) it was an unstable eigenmode. Second, the oblique waves, developing due to secondary instabilities, are the decaying eigenmodes, whereas in Craik (1971) these were growing waves.

Similarly to Craik (1971), we search for solution to the original 3D Navier-Stokes equations in the form of a superposition of three wave disturbances:

$$\begin{aligned} \phi = & \phi_0(z) + \Re\{A_0\psi_0(z) \exp[i(\omega t - kx)]\} \\ & + \Re\{\psi_1(z) \exp(i\omega_1 t)(A_+(t) \exp[-i(k_{1x}x + k_{1y}y)] \\ & + A_-(t) \exp[-i(k_{1x}x - k_{1y}y)])\}, \end{aligned} \quad (19)$$

where $\phi_0(z)$ stands for the vorticity, temperature or stream function of the undisturbed flow. The term in the first curly

brackets in Eq. (19) is the wave-induced disturbance of the air-flow with the amplitude A_0 , frequency ω and wavenumber k of the surface wave. ($\omega = kc$, where c is the phase velocity of the surface wave, $k = 2\pi$, and $c = 0.05$.) The terms in the second curly brackets account for the oblique wave disturbances with the frequency ω_1 , amplitudes A_{\pm} , and wavenumber vectors $\mathbf{k}_1 = (k_{1x}, k_{1y}) = (\pi, \pm 2\pi)$ (observed in the spectrum in Figure 4). Suppose that the frequency ω_1 and the wave numbers of the waves in the second term in Eq. (19), satisfy the conditions of parametric resonance:

$$\omega_1 = \frac{1}{2}(\omega + \Delta), \quad k_{1x} = \frac{1}{2}k \quad (20)$$

with a certain complex detuning Δ between the frequency of the surface wave, ω , and the complex frequency of the oblique wave, ω_1 . Here the real part of the detuning, $\Re\{\Delta\}$, describes the deviation of the frequencies ω_1 and ω from the exact resonance condition and the imaginary part $\Im\{\Delta\}$ is the oblique wave damping rate. Note that the imaginary part of the frequency ω_1 , $\Im\{\omega_1\} = \Im\{\Delta\}$, should be negative to keep the flow in the steady state. Similarly to Craik (1971), the original 3D equations are derived from the equations for complex amplitudes of the disturbances, A_0 and A_{\pm} using the perturbation method. The equations for A_+ and A_- read

$$\frac{dA_+}{dt} = \sigma A_0 A_-^* \exp(-i2t\Delta), \quad (21)$$

$$\frac{dA_-}{dt} = \sigma A_0 A_+^* \exp(-i2t\Delta) \quad (22)$$

whereas, in the considered case, A_0 does not depend on time. The change of variables $A_{\pm} = B_{\pm} \exp(-it\Delta)$ and simple algebra yields the equation for B_-

$$\frac{d^2 B_-}{dt^2} - 2\Im\{\Delta\} \frac{dB_-}{dt} + B_- (|\Delta|^2 - |\sigma A_0|^2) = 0. \quad (23)$$

Here, σ is a complex coefficient which, in principle, can be evaluated for the considered base flow characteristics. Provided that $|\sigma A_0| > |\Delta|$, Eq. (23) has the exponentially growing solution:

$$B_- \sim \exp(\lambda t), \quad \text{where } \lambda = \Im\{\Delta\} + \sqrt{|\sigma A_0|^2 - (\Re\{\Delta\})^2}. \quad (24)$$

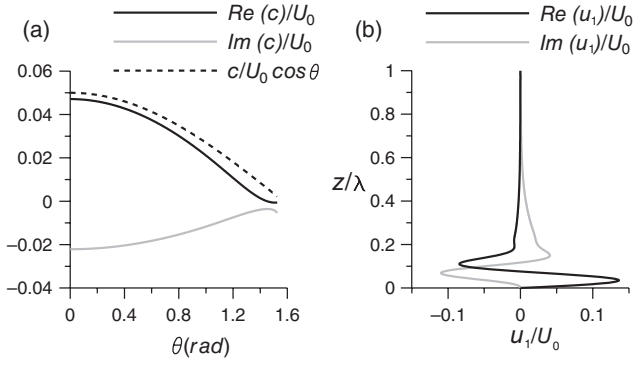


Figure 8. (a) Real and imaginary parts of the phase velocity of oblique wave as functions of the angle, θ , between the wave vector and the x -axis, and (b) vertical profiles of the real and imaginary parts of the horizontal velocity of the eigenfunction at $\mathbf{k}_1 = (\pi, 2\pi)$, for $Re = 15\,000$, $Ri = 0.08$, $ka = 0.2$, and $c/U_0 = 0.05$.

Evaluation of coefficient σ is beyond the scope of the present study. Let us consider only the dispersion characteristics of the oblique waves in the air-flow, and investigate whether these waves can be in resonance with the forced, wave-induced disturbance.

To obtain the dispersion relation for oblique harmonic waves, one needs to find a solution to the eigenvalue problem of the linearized 3D Navier-Stokes equations. The problem of oblique waves propagating in the plane-parallel flow can be reduced to the 2D problem by a rotation mapping (e.g. Drazin and Reid, 2004). Then the perturbations of the stream function, vorticity and temperature satisfy the following equations:

$$iK \left(\frac{d\psi_0}{d\eta} \chi_1 - \frac{d^3\psi_0}{d\eta^3} \psi_1 - \frac{g}{\Theta_0} \Theta_1 \right) = \nu \left(\frac{d^2\chi_1}{d\eta^2} - K^2 \chi_1 \right),$$

$$\frac{d^2\psi_1}{d\eta^2} - K^2 \psi_1 = -\chi_1,$$

$$iK \left(\frac{d\psi_0}{d\eta} \Theta_1 - \frac{d\Theta}{d\eta} \psi_1 \right) = \frac{\nu}{Pr} \left(\frac{d^2\Theta_1}{d\eta^2} - K^2 \Theta_1 \right), \quad (25)$$

where $d\Psi_0/dz = U(z)\cos\theta - C$, $\theta = \arctan(k_{1y}/k_{1x})$ is the angle between the x -axis and the wavenumber vector of the oblique wave, $K = (k_{1x}^2 + k_{1y}^2)^{1/2}$ is the absolute value of the wavenumber of the oblique wave; and C is the phase velocity of the oblique wave. The resonance conditions (20) require the following relationships between the parameters of the wave-induced disturbance and the oblique wave:

$$k = 2K \cos\theta, \quad C = c \cos\theta + \frac{\Delta}{2K}. \quad (26)$$

The system (25) was solved numerically for the mean velocity and temperature profiles, $U(\eta)$ and $\Theta(\eta)$, obtained in DNS for $Re = 15\,000$, $Ri = 0.08$, $ka = 0.2$, and $c/U_0 = 0.05$. Taking the zero boundary conditions for disturbances of vertical and horizontal velocity and temperature at $z=0$ and $z/\lambda = 1$, we determined the eigenfunctions and eigen-frequencies for the oblique wave satisfying the condition of resonance with the wave-induced disturbance, $K = \pi/\cos\theta$. Figure 8(a) shows the real and imaginary parts of the phase velocity C of this wave versus θ . The real part of the detuning of the phase velocity from the phase velocity of the wave-induced disturbance is significantly smaller than the imaginary part. This means that the condition for the growth of the oblique wave has the form $|\sigma A_0| > |\text{Im}\{\Delta\}|$, i.e. the growth rate of the parametric instability must exceed the linear damping rate of the eigenmode. This explains the threshold in the dependence of the magnitude of fluctuations of velocity and temperature on the wave slope in Figure 1(a).

Figure 8(b) shows vertical profiles of real and imaginary parts of the eigenfunction of horizontal disturbance velocity, u_1 , localized near the surface, which agrees well with DNS which reveals disturbances also localized in the vicinity of the waved surface.

The linear theory does not explain the line spectrum of the excited oblique waves, since the function $C(\theta)$ shown in Figure 8 does not have sharp peaks. Then the occurrence of the unstable mode with $k_{1y} = 2\pi$ in DNS (Figure 4) can be related to the details of dependence of the coefficient σ on the air-flow parameters; this is not considered in the present article.

Note also that the proposed model considers the 2D disturbances of the vorticity, streamfunction and temperature forced by the surface wave (cf. Eq. (12)). Since the model is based on the linearized Navier-Stokes equations averaged in the spanwise (y) direction, it cannot reproduce either the effect of subharmonics generation or the development of the spanwise instability of the flow. Thus, it cannot reproduce the features of the vorticity field distribution in Figure 2. Nevertheless, it correctly predicts the profiles of the velocity and temperature rms fluctuations observed in DNS in Figure 5. That means that the contribution of the forced 2D disturbance is dominant in the considered case.

4. Conclusions

We performed direct numerical simulation of stably stratified air-flows over a waved water surface with particular attention to supercritically stable stratifications. At sufficiently small wave slopes, the supercritically stratified flows become laminar, similar to the analogous strongly stratified flows over a flat solid surface. However, if the wave slope exceeds some threshold value, the velocity and temperature fluctuations are maintained even in supercritically stratified flows in the vicinity of the critical level, where the wave phase velocity coincides with the mean flow velocity. We propose for this phenomenon the name ‘wave-induced pre-turbulence’.

We propose also a theoretical model explaining the development of pre-turbulent motions as a result of generation of 2D disturbances in the air-flow over the surface wave. The theoretically predicted amplitudes of the wave-induced 2D disturbances in the air-flow are in good qualitative and quantitative agreement with DNS. These disturbances are subject to the development of a secondary instability along the wave-front direction. Our theoretical model explains the development of this instability as a result of a parametric resonance between the 2D disturbance induced in the air-flow by the surface wave and oblique waves. This mechanism is similar to the one suggested by Craik (1971) for the explanation of turbulent transition in the boundary-layer flow. Our DNS results show also that increasing the bulk Reynolds number leads to the development of a wider spectrum of the disturbance flow and a possible further transition to a developed turbulent regime.

The regime of pre-turbulent, wave-induced motions, discussed in the present article, is expected to be observed in laboratory conditions for wind speeds of the order $U_0 = O(1 \text{ m s}^{-1})$ above water surface waves with wavelength $\lambda = O(1 \text{ m})$ and warm air versus cold water temperature difference about $\Delta\Theta = O(10 \text{ K})$. A similar situation also occurs in the field when warm air is advected from a heated land surface over a cold sea, e.g. Melas (1989) reports observations of $\Delta\Theta$ about 10 K at 1.3 m in Oresund region in June. Under these conditions, the bulk Reynolds and Richardson numbers, defined in Eqs (2) and (3), are found to be quite close to these numbers in our DNS.

We have demonstrated that the wave-induced pre-turbulent motions exhibit the higher energy and, the larger the bulk Reynolds number, the wider is the spectrum of wave-induced motions. In view of this conclusion, it is only natural to expect a transition from wave-induced pre-turbulence to the real turbulence at sufficiently large Reynolds numbers, for given supercritical Richardson numbers. Similar physical mechanisms of the maintenance of very high Re , supercritically stratified turbulence are revealed in the Energy and Flux-Budget (EFB) turbulence closure theory (Zilitinkevich *et al.*, 2013).

Acknowledgements

We are grateful to the anonymous referees for all comments and suggestions.

This work is supported by the grant of the government of the Russian Federation (contract 11.G34.31.0048), Federal Targeted Program 'Scientific and Pedagogical Staff for Innovative Russia' for 2009–2013, by Contract No. 14.578.21.0033 (2014–2016); the European Commission ERC-Ideas PoC Project 632295-INMOST (2014–2015); the Academy of Finland project 'Atmosphere-hydrosphere interaction in the Baltic Basin and Arctic Seas' ABBA, Contract No. 280700 (2014–2017); RFBR (Nos. 14-05-00367, 13-05-00865, 14-05-91767, 15-35-20953). Theoretical analysis and DNS were supported by the Russian Science Foundation (Nos. 14-17-00667 and 15-17-20009, respectively). YIT was partially supported by FP7 collaborative Project No. 612610.

References

- Craik ADD. 1971. Non-linear resonant instability in boundary layers. *J. Fluid Mech.* **50**: 393–413, doi: 10.1017/S0022112071002635.
- Drazin PG, Reid WH. 2004. *Hydrodynamic Stability*. Cambridge University Press: Cambridge, UK.
- Druzhinin OA, Troitskaya YI, Zilitinkevich SS. 2015. Stably stratified air flow over wavy water surface. Part 1: Stationary turbulent regimes. *Q. J. R. Meteorol. Soc.*, doi: 10.1002/qj.2677.
- Flores O, Riley JJ. 2011. Analysis of turbulence collapse in the stably stratified surface layer using direct numerical simulation. *Boundary-Layer Meteorol.* **139**: 241–259, doi: 10.1007/s10546-011-9588-2.
- Melas D. 1989. The temperature structure in a stably stratified internal boundary layer over a cold sea. *Boundary-Layer Meteorol.* **48**: 361–375.
- Troitskaya YI, Ezhova EV, Zilitinkevich SS. 2013a. Momentum and buoyancy transfer in atmospheric turbulent boundary layer over wavy water surface. Part 1: Harmonic wave. *Nonlinear Proc. Geophys.* **20**: 825–839, doi: 10.5194/npg-20-825-2013.
- Troitskaya YI, Ezhova EV, Sergeev DA, Kandaurov AA, Baidakov GA, Vdovin MI, Zilitinkevich SS. 2013b. Momentum and buoyancy transfer in atmospheric turbulent boundary layer over wavy water surface. Part 2. Wind wave spectra. *Nonlinear Proc. Geophys.* **20**: 841–856, doi: 10.5194/npg-20-841-2013.
- Zilitinkevich SS, Elperin T, Kleerorin N, Rogachevskii I, Esau IN. 2013. A hierarchy of energy- and flux-budget (EFB) turbulence closure models for stably stratified geophysical flows. *Boundary-Layer Meteorol.* **146**: 341–373, doi: 10.1007/s10546-012-9768-8.